Enhanced Proton Conductivity in a Layered Coordination Polymer

Ricardo F. Mendes,[1,†]* Paula Barbosa,[2,†] Eddy M. Domingues,[2] Patrícia Silva,[1] Filipe Figueiredo,[2]* Filipe A. Almeida Paz[1]*

A contribution from

[1]*Department of Chemistry, CICECO – Aveiro Institute of Materials, University of Aveiro, 3810-193 Aveiro, Portugal*

[2]*Department of Materials & Ceramic Engineering, CICECO – Aveiro Institute of Materials, University of Aveiro, 3810-193 Aveiro, Portugal*

Supporting Information

Table of Contents

1. Materials and Methods S3
2. Synthesis optimization and crystal morphology: $[Gd_2(H_3nmp)_2]\cdot xH_2O$ (2) (x = 1 to 4).....S5
3. Additional Characterization of $[Gd_2(H_3nmp)_2]\cdot xH_2O$ (2) (x = 1 to 4) S7
4. Structural Elucidation and Transformation.....S7
4.1. Experimental.....S7
4.2. Structural features of $[Gd_2(H_3nmp)_2]\cdot 1.4H_2O$ (2sc) S13
5. Protonic conductivity and water vapor sorption isotherms S15
5.1. Experimental.....S15
5.2. Protonic conductivity and water sorption Studies S15
References.....S22

1. Materials and Methods

General Instrumentation. Thermogravimetric analyses (TGA) were carried out using a Shimadzu TGA 50 from ambient temperature to *ca*. 800 ºC (heating rate of 5 ºC/min) under a continuous stream of air at a flow rate of 20 mL min^{-1}. Fourier Transform Infrared (FT-IR) spectra in the range 4000-350 cm^{-1} were recorded as KBr pellets (2 mg of sample was mixed in a mortar with 200 mg of KBr) using a Bruker Tensor 27 spectrometer by averaging 256 scans at a maximum resolution of 2 cm^{-1}. Elemental analyses for C, N and H were performed with a Truspec Micro CHNS 630-200-200 elemental analyser at the Department of Chemistry, University of Aveiro. Analysis parameters: sample amount between 1 and 2 mg; combustion furnace temperature = 1075 ºC; after burner temperature = 850 ºC. Detection method: carbon - infrared absorption; hydrogen - infrared absorption; nitrogen – infrared absorption. Analysis time = 4 minutes. Gases required: carrier – helium; combustion – oxygen; pneumatic – compressed air. Routine Powder X-Ray Diffraction (PXRD) data for all prepared materials were collected at ambient temperature on a Empyrean PANalytical diffractometer (Cu $K_{a1,2}$ X-radiation, λ_1 = 1.540598 Å; λ_2 = 1.544426 Å), equipped with an PIXcel 1D detector and a flat-plate sample holder in a Bragg-Brentano para-focusing optics configuration (45 kV, 40 mA). Intensity data were collected by the step-counting method (step 0.01º), in continuous mode, in the *ca*. $3.5 \leq 2\theta \leq 50º$ range. PXRD patterns were collected under variable temperature and relative humidity on a Bruker D8 ADVANCE diffractometer (Johansson X-ray monochromator for Mo K_{a1} X-radiation, λ_1 = 0.70930 Å) equipped with a multi-sample humidity chamber Anton Paar MHC trans and a LYNXEYE XE detector (50 kV, 50 mA), at the *Servicios Centralizados de Apoyo a la Investigación*, University of Málaga.

Reagents. Chemicals were readily available from commercial sources and were used as received without further purification. For all tested synthetic methods, gadolinium (III) chloride hydrate (at least 99% of purity, Sigma-Aldrich) was employed as the metallic precursor in the optimization of the reaction parameters. Gadolinium (III) oxide was used for the microwave-assisted and one-pot syntheses (at least 99.99%, Jinan Henghua Sci. & Tec. Co. Ltd). Nitrilotris(methylenephosphonic acid) (H_6nmp, $N(CH_2PO_3H_2)_3$, 97%) and hydrochloric acid (HCl, 37% Analytical Reagent Grade) were purchased from Fluka and Fisher Chemical, respectively.

Preparation of $[Gd(H_4nmp)(H_2O)_2]Cl{\cdot}2H_2O$ (1)

The compound was prepared following a reported procedure.[1] In a typical synthesis, a mixture containing H_6nmp (0.1425 g, 0.477 mmol) and Gd_2O_3 (0.1587 g, 0.438 mmol) in *ca.* 10.0 mL of distilled water and 10.0 mL of HCl 6 M was stirred thoroughly in a round bottom flask. The resulting solution was

kept at 120 ºC for 18h in an oil bath, after which the vessel was allowed to cool slowly to ambient temperature. Crystalline material was readily obtained after *ca*. 15 min.

Preparation of $[Gd_2(H_3nmp)_2]\cdot xH_2O$ (2) (x = 1 to 4)

Hydrothermal synthesis (**2ht**): A suspension containing H_6nmp (0.153 g, 0.512 mmol) and $GdCl_3\cdot 6H_2O$ (0.190 g, 0.512 mmol) in *ca.* 15.0 mL of distilled water (molar ratio of about 1 : 1 : 650) was stirred thoroughly in open air (at ambient temperature) for five minutes. The resulting homogeneous suspension was transferred to an adapted Teflon-lined Parr Instruments reaction vessel (autoclave with internal volume of *ca.* 24 mL), which was then placed inside a custom preheated oven at 120 ºC for 48h. After reacting, the vessels were allowed to cool to ambient temperature inside the oven. The contents of the autoclaves were formed by a white suspension, with the final product being recovered by vacuum filtration, washed with copious amounts of distilled water, air-dried.

Microwave-assisted hydrothermal synthesis (**2mw**): A reactive mixture with identical chemical composition to that described for the typical hydrothermal approach using convection heating was stirred thoroughly in open air for five minutes. The resulting homogeneous suspension was transferred to a 10 mL IntelliVent reactor that was placed inside a CEM Focused Microwave™ Synthesis System Discover S-Class equipment. Reactions took place with constant magnetic stirring (controlled by the microwave equipment) at 120 ºC for 10 min. A constant flow of air (*ca.* 10 bar of pressure) ensured a close control of the temperature inside the vessel. After reacting, a white suspension was obtained, and the final product was recovered by vacuum filtration, followed by washing with copious amounts of distilled water, and then air-dried overnight.

One-Pot synthesis (**2op**): A reactive mixture with identical chemical composition to that described for the typical hydrothermal approach using convection heating was prepared in a round bottom flask and heated to 120 ºC and maintained for 48h. After reacting, the vessels were allowed to cool slowly to ambient temperature and the final product was recovered by vacuum filtration, followed by washing with copious amounts of distilled water, and then air-dried overnight.

Elemental composition for representative as-prepared $[Gd_2(H_3nmp)_2]\cdot 2H_2O$: *Calculated C 7.65, H 2.35, N 2.97. Found: C 7.47, H 2.31, N 2.91.* ***Selected FT-IR data (in cm^{-1}) for the isotypical series of compound $[Gd_2(H_3nmp)_2]\cdot 2H_2O$:*** *$\nu(H_2O)_{coord}$ = 3500 w; ν(N–H) = 3005 w, $\nu_{sym+asym}$(C–H) = 2845, 2777, 2747, 2660 w; ν(P−OH) = 2325 w; $\delta(H_2O)$ = 1630 w; $\delta(P-CH_2)$ = 1482, 1428, 1402, 1328 m; ν(P=O) = 1208, 1172 m-vs; $\nu((CH_2)_3\text{-}N)$ = 1120 (shoulder), 1099, 1070, 1047 vs; ν(P−O) = 1005, 988, 945, 913 m; ν(P−C) = 808, 753, 723 m.* ***Thermogravimetric analysis (TGA) data (weight losses in %) and derivative***

thermogravimetric peaks (DTG; in italics inside the parentheses) for [Gd$_2$(H$_3$nmp)$_2$]·2H$_2$O: *15–140ºC -3.9% (59ºC), 350ºC–425ºC -1.6% (408ºC), 425–620ºC -4.4% (460ºC), 620–800ºC -3.3%.*

2. Synthesis optimization and crystal morphology: [Gd$_2$(H$_3$nmp)$_2$]·*x*H$_2$O (2) (*x* = 1 to 4)

Besides the *in situ* formation of [Gd$_2$(H$_3$nmp)$_2$]·*x*H$_2$O (**2**) inside the climate chamber, the material was directly prepared by three different experimental methods: hydrothermal, microwave-assisted and one-pot syntheses (see Experimental Section in the main paper for additional details). Optimization of each synthetic approach revealed that **2** could be obtained from a myriad of distinct conditions:

i) Using static hydrothermal synthesis (convection heating), poorly crystalline **2** could be isolated after just a few hours of reaction (*e.g.*, 2h at 140 ºC or 1h at 190 ºC). Crystallinity could be slightly improved using longer reaction periods, but for very long periods the crystals are destroyed (*e.g.*, 4 days at 140 ºC or 2 days at 190 ºC).

ii) Using microwave-assisted synthesis (MWAS), for temperatures lower than *ca.* 100 ºC amorphous compounds are isolated and at *ca.* 140 ºC physical mixtures of **2** with [Gd(H$_3$nmp)][2] are obtained. For this latter temperature, decreasing the irradiation power to, *e.g.* 50 W, **2** is isolated as a pure phase (*please note*: a careful combination of irradiation power and the time for the heating ramp needs to be adjusted). In the MWAS the time of reaction plays a decisive role in the isolation of **2**. The optimal conditions to isolate **2** within 10 minutes correspond to a temperature of *ca.* 100-120 ºC and an irradiation power of *ca.* 100 W.

iii) Using the one-pot method, poorly crystalline **2** can be isolated at lower temperatures (*e.g.*, refluxing at 80 ºC for 12h). Slightly larger crystals of **2** were isolated using this method by replacing the metal source (chloride for the oxide) and including HCl in the reactive medium.

Crystals of [Gd$_2$(H$_3$nmp)$_2$]·*x*H$_2$O (**2**) (*x* = 1 to 4) present a plate-like morphology for a wide range of conditions with individual crystallites being stacked into aggregates with different shapes (Figure 1 in the main paper). In all synthetic approaches the crystals are regular thin plates (in the nanometer range) which grow uniformly in the matrix, without the presence of precipitates (or other defects). For the case of the typical hydrothermal approach, the formed thin petal-like crystallites aggregate giving rise to well defined spherical agglomerates. Similar thin petal-like crystals were obtained when using MWAS but, unlike the typical hydrothermal reaction, the agglomeration of particles gave rise to clusters of irregular shapes. The one-pot method yielded a larger variety of morphologies for which we observed typically the presence of two-dimensional rectangular particles of **2** with variable length attaining around 10 μm with the concomitant increase in the crystallite thickness.

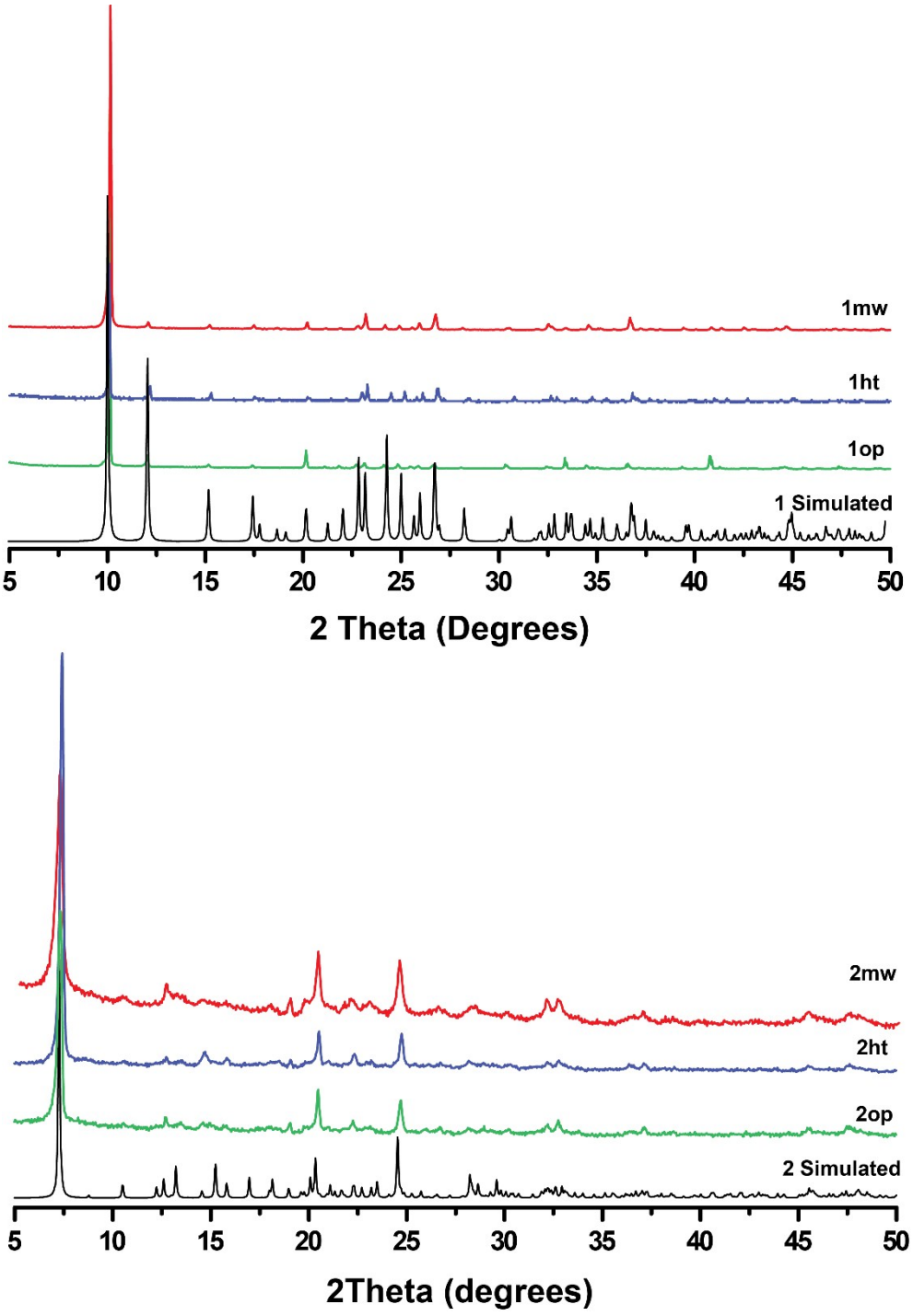

Figure S1. Powder X-ray diffraction of $[Gd(H_4nmp)(H_2O)_2]Cl{\cdot}2H_2O$ (**1**) and $[Gd_2(H_3nmp)_2]{\cdot}xH_2O$ (**2**) (x = 1 to 4) obtained by hydrothermal (**ht**), microwave (**mw**) and one-por (**op**) syntheses.

3. Additional Characterization of $[Gd_2(H_3nmp)_2]\cdot xH_2O$ (2) (x = 1 to 4)

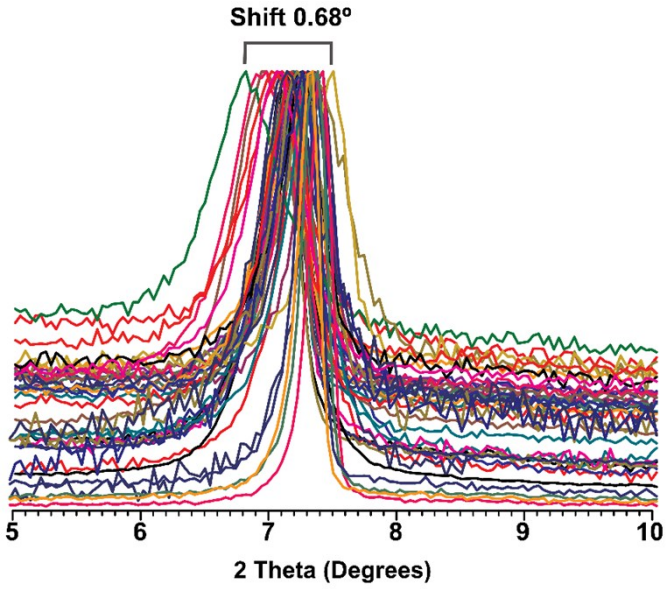

Figure S2. Collection of a total of 40 powder X-ray diffraction patterns of representative samples of $[Gd_2(H_3nmp)_2]\cdot xH_2O$ (**2**) (x = 1 to 4) depicting the reflection attributed to the (002) Miller plane. The Figure depicts a significant shift for this reflection among all represented samples which cannot be attributed to just any instrumental error or zero shift.

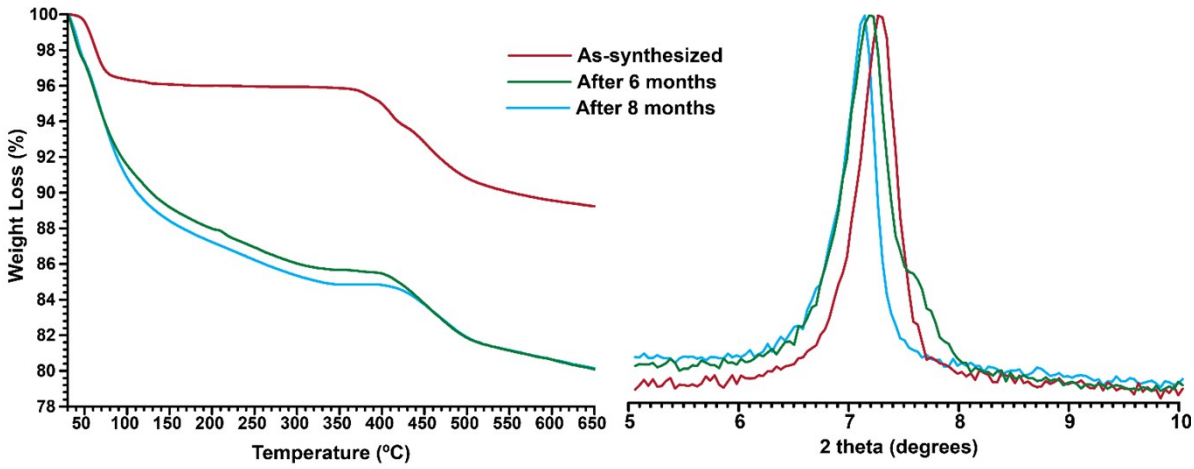

Figure S3. Thermograms and the corresponding powder X-ray diffraction patterns for the (002) Miller plane of a sample of $[Gd_2(H_3nmp)_2]\cdot xH_2O$ (**2**) (x = 1 to 4) immediately after synthesis (in red), after 6 months (in green) and after 8 months (in blue) when stored in normal conditions.

4. Structural Elucidation and Transformation

4.1. Experimental

The one-pot reaction approach allowed, after many attempts, the isolation of a single colourless block-like crystal which was manually harvested from the reaction vial. The crystal was immersed in highly viscous FOMBLIN Y perfluoropolyether vacuum oil (LVAC 140/13, Sigma-Aldrich) to avoid degradation

or transformation caused by any evaporation or capture of solvent.[3] The crystal was mounted on a MiTeGen MicroLoop with the help of a Stemi 2000 stereomicroscope equipped with Carl Zeiss lenses.

X-ray diffraction data for **2sc** were collected at 180(2)K on a Bruker D8 QUEST equipped with Mo Kα sealed tube (λ = 0.71073 Å), a multilayer TRIUMPH X-ray mirror, a PHOTON 100 CMOS detector controlled by the APEX3 software package[4] and equipped with an Oxford Cryosystems Series 700 cryostream.[5] Diffraction images were processed using the software package SAINT+,[6] and data were corrected for absorption by the multiscan semi-empirical method implemented in SADABS 2016/2.[7]

The structure was solved using the algorithm implemented in SHELXT-2014/5,[8] which allowed the immediate location of almost all of the heaviest atoms composing the molecular unit. The remaining missing and misplaced non-hydrogen atoms were located from difference Fourier maps calculated from successive full-matrix least-squares refinement cycles on F^2 using the latest SHELXL from the 2018/3 release.[9] All structural refinements were performed using the graphical interface ShelXle.[10]

Hydrogen atoms bound to carbon (namely the $–CH_2–$ groups) and nitrogen were placed at their idealized positions using the *HFIX 23* or *HFIX 13* in SHELXL-2014. All hydrogen atoms were included in subsequent refinement cycles with isotropic thermal displacements parameters (U_{iso}) fixed at $1.2\times U_{eq}$ of the parent atoms. Hydrogen atoms associated with the water molecules, both of crystallization and coordinated to La^{3+}, could not be located from difference Fourier maps and no attempts were made to place them in calculated positions. These atoms were, however, included in the empirical formula of the compound (Table S1). Hydrogen atoms associated with the terminal P–OH groups were placed in calculated positions using the *HFIX 147* instruction in SHELXL-2014. To find which groups should be protonated it was necessary to simultaneously take into account the P–O bond lengths and the possibility of forming hydrogen bonds with neighbouring moieties. These hydrogen atoms were included in the final structural model by assuming isotropic thermal displacements behaviours with U_{iso} fixed at $1.5\times U_{eq}$ of the parent oxygen atoms.

The last difference Fourier map synthesis showed for **2sc**, the highest peak (4.74 $eÅ^{-3}$) and the deepest hole (-2.33 $eÅ^{-3}$) located at 1.48 and 1.07 Å from Gd2 and Gd1, respectively. Structural drawings have been created using the software package Crystal Impact Diamond.[11]

Crystallographic data (including structure factors) for the crystal structure of compound **2** have been deposited with the Cambridge Crystallographic Data Centre as supplementary publication data No. CCDC-1960178. Copies of the data can be obtained free of charge on application to CCDC, 12 Union Road, Cambridge CB2 2EZ, U.K. FAX: (+44) 1223 336033. E-mail: deposit@ccdc.cam.ac.uk.

Table S1. Crystal data collection and structure refinement details for $[Gd_2(H_3nmp)_2]\cdot 1.4H_2O$ (**2sc**).

Formula	$C_6H_{20.80}Gd_2N_2O_{19.40}P_6$
Formula weight	931.77
Temperature / K	180(2)
Crystal system	Triclinic
Space group	*P*-1
a / Å	9.7560(17)
b / Å	10.186(2)
c / Å	12.840(3)
α / º	98.371(7)
β / º	106.552(6)
γ / º	90.234(6)
Volume / Å^3	1208.6(4)
Z	2
ρ_{calc} / g cm^{-3}	2.560
μ(Mo Kα) / mm^{-1}	5.926
Crystal type	Colourless plate
Crystal size / mm	0.08×0.04×0.02
θ range (°)	3.64 – 25.34
Index ranges	$-11 \le h \le 10$
	$-12 \le k \le 11$
	$-15 \le l \le 15$
Collected Reflections	13319
Independent Reflections	3814 (R_{int} = 0.0515)
Completeness to θ = 25.24	86.8%
Final *R* indices [$I > 2\sigma(I)$]	*R*1 = 0.1075
	*wR*2 = 0.2641
Final *R* indices (all data)	*R*1 = 0.1526
	*wR*2 = 0.2833
Largest diff. peak and hole /eÅ^{-3}	4.74 and -2.33

[a] $R1 = \sum \left| |F_o| - |F_c| \right| / \sum |F_o|$

[b] $wR2 = \sqrt{\sum \left[w\left(F_o^2 - F_c^2\right)^2 \right] / \sum \left[w\left(F_o^2\right)^2 \right]}$

[c] $w = 1/\left[\sigma^2\left(F_o^2\right) + \left(mP\right)^2 + nP \right]$ where $P = \left(F_o^2 + 2F_c^2\right)/3$

Table S2. Selected bond lengths (in Å) and angles (in degrees) for the two crystallographically independent Gd^{3+} coordination environments present in $[Gd_2(H_3nmp)_2]\cdot 1.4H_2O$ (**2sc**).[a]

Gd1—O9^{i}	2.19 (3)	Gd1—O10^{iii}	2.42 (2)
Gd1—O4	2.26 (3)	Gd1—O11	2.456 (19)
Gd1—O1	2.27 (2)	Gd1—O10	2.46 (2)
Gd1—O17^{ii}	2.27 (2)	Gd2—O18^{iv}	2.28 (2)
Gd2—O13	2.29 (2)	Gd2—O12^{iv}	2.29 (2)
Gd2—O6^{v}	2.31 (2)	Gd2—O2^{vi}	2.37 (2)
Gd2—O3	2.44 (2)	Gd2—O2	2.51 (2)
O9^{i}—Gd1—O4	100.2 (10)	O9^{i}—Gd1—O1	169.8 (10)
O4—Gd1—O1	83.9 (8)	O9^{i}—Gd1—O17^{ii}	83.6 (10)
O4—Gd1—O17^{ii}	78.0 (8)	O1—Gd1—O17^{ii}	88.1 (8)
O9^{i}—Gd1—O10^{iii}	88.7 (9)	O4—Gd1—O10^{iii}	78.8 (8)
O1—Gd1—O10^{iii}	101.3 (8)	O17^{ii}—Gd1—O10^{iii}	153.9 (8)
O9^{i}—Gd1—O11	92.3 (9)	O4—Gd1—O11	153.0 (8)
O1—Gd1—O11	80.3 (7)	O17^{ii}—Gd1—O11	79.7 (7)
O10^{iii}—Gd1—O11	125.7 (7)	O9^{i}—Gd1—O10	79.6 (9)
O4—Gd1—O10	147.3 (8)	O1—Gd1—O10	102.2 (7)
O17^{ii}—Gd1—O10	133.7 (8)	O10^{iii}—Gd1—O10	68.5 (8)
O11—Gd1—O10	58.4 (6)	O18^{iv}—Gd2—O13	101.6 (9)
O18^{iv}—Gd2—O12^{iv}	84.8 (8)	O13—Gd2—O12^{iv}	166.1 (8)
O18^{iv}—Gd2—O6^{v}	76.5 (8)	O13—Gd2—O6^{v}	81.5 (9)
O12^{iv}—Gd2—O6^{v}	88.1 (8)	O18^{iv}—Gd2—O2^{vi}	79.6 (8)
O13—Gd2—O2^{vi}	91.0 (8)	O12^{iv}—Gd2—O2^{vi}	102.4 (8)
O6^{v}—Gd2—O2^{vi}	152.8 (8)	O18^{iv}—Gd2—O3	153.0 (8)
O13—Gd2—O3	89.5 (8)	O12^{iv}—Gd2—O3	79.7 (8)
O6^{v}—Gd2—O3	81.0 (8)	O2^{vi}—Gd2—O3	125.3 (7)
O18^{iv}—Gd2—O2	146.8 (8)	O13—Gd2—O2	81.6 (8)
O12^{iv}—Gd2—O2	99.9 (8)	O6^{v}—Gd2—O2	136.1 (7)
O18^{iv}—Gd2—O3	153.0 (8)	O13—Gd2—O3	89.5 (8)
O12^{iv}—Gd2—O3	79.7 (8)	O6^{v}—Gd2—O3	81.0 (8)
O2^{vi}—Gd2—O3	125.3 (7)	O18^{iv}—Gd2—O2	146.8 (8)
O13—Gd2—O2	81.6 (8)	O12^{iv}—Gd2—O2	99.9 (8)
O6^{v}—Gd2—O2	136.1 (7)	O2^{vi}—Gd2—O2	67.3 (8)
O3—Gd2—O2	58.7 (7)		

[a] Symmetry transformations used to generate equivalent atoms: (i) x, $y+1$, z; (ii) $-x$, $-y+2$, $-z+1$; (iii) $-x+1$, $-y+2$, $-z+1$; (iv) x, $y-1$, z; (v) $-x+1$, $-y+1$, $-z+1$; (vi) $-x$, $-y+1$, $-z+1$.

Table S3. Fractional atomic coordinates and isotropic or equivalent isotropic displacement parameters (Å^2) of $[Gd_2(H_3nmp)_2]\cdot 1.4H_2O$ (**2sc**).

Atom	*x*	*y*	*z*	U_{iso}*/U_{eq}
Gd1	0.43729 (16)	0.92186 (16)	0.61560 (14)	0.0182 (5)
Gd2	0.06218 (16)	0.37937 (16)	0.38290 (14)	0.0184 (5)
P1	0.2823 (9)	0.5861 (8)	0.5405 (7)	0.0171 (19)
P2	0.7092 (9)	0.7244 (9)	0.7861 (8)	0.023 (2)
P3	0.5110 (10)	0.2604 (10)	0.7681 (8)	0.029 (2)
P4	0.2153 (8)	1.0713 (8)	0.4597 (7)	0.0154 (18)
P5	−0.0024 (10)	0.6650 (10)	0.2273 (9)	0.031 (2)
P6	−0.2129 (9)	1.1186 (9)	0.2099 (8)	0.022 (2)
O1	0.328 (2)	0.723 (2)	0.5269 (18)	0.017 (5)
O2	0.127 (2)	0.571 (2)	0.5373 (18)	0.019 (5)
O3	0.307 (2)	0.474 (2)	0.4570 (18)	0.018 (5)
O4	0.602 (3)	0.795 (2)	0.711 (2)	0.032 (6)
O5	0.749 (3)	0.796 (3)	0.905 (2)	0.034 (6)
H5	0.681870	0.843230	0.914156	0.051*
O6	0.849 (2)	0.704 (2)	0.761 (2)	0.026 (6)
O7	0.645 (3)	0.291 (3)	0.866 (2)	0.041 (7)
H7	0.697023	0.349935	0.854689	0.062*
O8	0.385 (3)	0.301 (3)	0.809 (3)	0.054 (8)
O9	0.510 (3)	0.118 (3)	0.712 (3)	0.049 (8)
O10	0.373 (2)	1.062 (2)	0.4696 (18)	0.015 (5)
O11	0.192 (2)	0.9914 (19)	0.5450 (16)	0.012 (4)
O12	0.171 (2)	1.213 (2)	0.4735 (19)	0.023 (5)
O13	0.004 (3)	0.549 (2)	0.281 (2)	0.028 (6)
O14	−0.139 (4)	0.656 (3)	0.128 (3)	0.061 (9)
H14	−0.121837	0.694236	0.079323	0.092*
O15	0.122 (3)	0.703 (3)	0.192 (3)	0.055 (8)
O16	−0.257 (3)	1.140 (3)	0.086 (2)	0.032 (6)
H16	−0.345444	1.149838	0.064221	0.049*
O17	−0.350 (2)	1.106 (2)	0.2425 (19)	0.024 (5)
O18	−0.105 (2)	1.217 (2)	0.283 (2)	0.026 (6)
N1	0.529 (3)	0.506 (3)	0.689 (2)	0.023 (7)
H1	0.561816	0.535938	0.628541	0.027*
N2	−0.030 (3)	0.940 (3)	0.314 (2)	0.021 (6)
H2	−0.061334	0.992348	0.374291	0.025*
C1	0.381 (3)	0.562 (3)	0.674 (3)	0.020 (7)
H1A	0.392433	0.648219	0.723217	0.025*
H1B	0.323159	0.501071	0.700497	0.025*

C2	0.635 (4)	0.563 (3)	0.788 (3)	0.027 (8)
H2A	0.714028	0.501922	0.803561	0.033*
H2B	0.591464	0.570312	0.849339	0.033*
C3	0.527 (4)	0.357 (3)	0.666 (3)	0.026 (8)
H3A	0.615992	0.332441	0.646906	0.031*
H3B	0.446382	0.327501	0.598815	0.031*
C4	0.117 (4)	0.992 (4)	0.321 (3)	0.028 (8)
H4A	0.107889	1.057681	0.269391	0.033*
H4B	0.171573	0.918060	0.296788	0.033*
C5	−0.026 (4)	0.794 (3)	0.330 (3)	0.025 (8)
H5A	−0.117046	0.771577	0.345086	0.030*
H5B	0.051503	0.788027	0.398480	0.030*
C6	−0.138 (4)	0.957 (3)	0.204 (3)	0.023 (8)
H6A	−0.215517	0.887263	0.184487	0.027*
H6B	−0.088997	0.945307	0.145122	0.027*
O1W	0.554 (4)	0.826 (4)	1.000 (3)	0.052 (10)*
O2W	0.946 (6)	0.174 (6)	0.001 (5)	0.066 (16)*

Table S4. Hydrogen bonding geometry (distances in Å and angles in degrees) for $[Gd_2(H_3nmp)_2]\cdot 1.4H_2O$ (**2sc**).[a]

D–H···A[a]	*d*(D···A)	<(DHA)
O5—H5···O1*W*	2.53 (5)	130
O7—H7···O15^{v}	2.59 (4)	119
O14—H14···O5^{vii}	3.30 (4)	142
O16—H16···O1*W*^{ii}	2.84 (5)	175
N1—H1···O3^{v}	2.81 (4)	150
N2—H2···O11^{ii}	2.75 (3)	148

[a] Symmetry transformations used to generate equivalent atoms: (ii) −*x*, −*y*+2, −*z*+1; (v) −*x*+1, −*y*+1, −*z*+1; (vii) *x*−1, *y*, *z*−1

4.2. Structural features of $[Gd_2(H_3nmp)_2]\cdot 1.4H_2O$ (2sc)

Compound **2sc**, formulated as $[Gd_2(H_3nmp)_2]\cdot 1.4H_2O$ on the basis of single-crystal X-ray diffraction (see Tables S1 to S4), crystallizes in the triclinic space group *P*-1, with the asymmetric unit being composed of two heptacoordinated $Gd^{3+}$and two H_3nmp^{3-} organic linkers as depicted in Figure S2.

The two Gd^{3+} centres are both coordinated to a total six phosphonate groups arising from five symmetry-related H_3nmp^{3-} organic linkers, with the coordination polyhedron resembling a distorted pentagonal bipyramid. H_3nmp^{3-} acts as a pentadentate linker, connecting the two independent metal centres to another three symmetry-related ones. This high connectivity allows the formation of an infinite neutral compact layer and, as observed for other related compounds, it is responsible for the trapping of Gd^{3+} centres inside a phosphonic-type inorganic matrix.

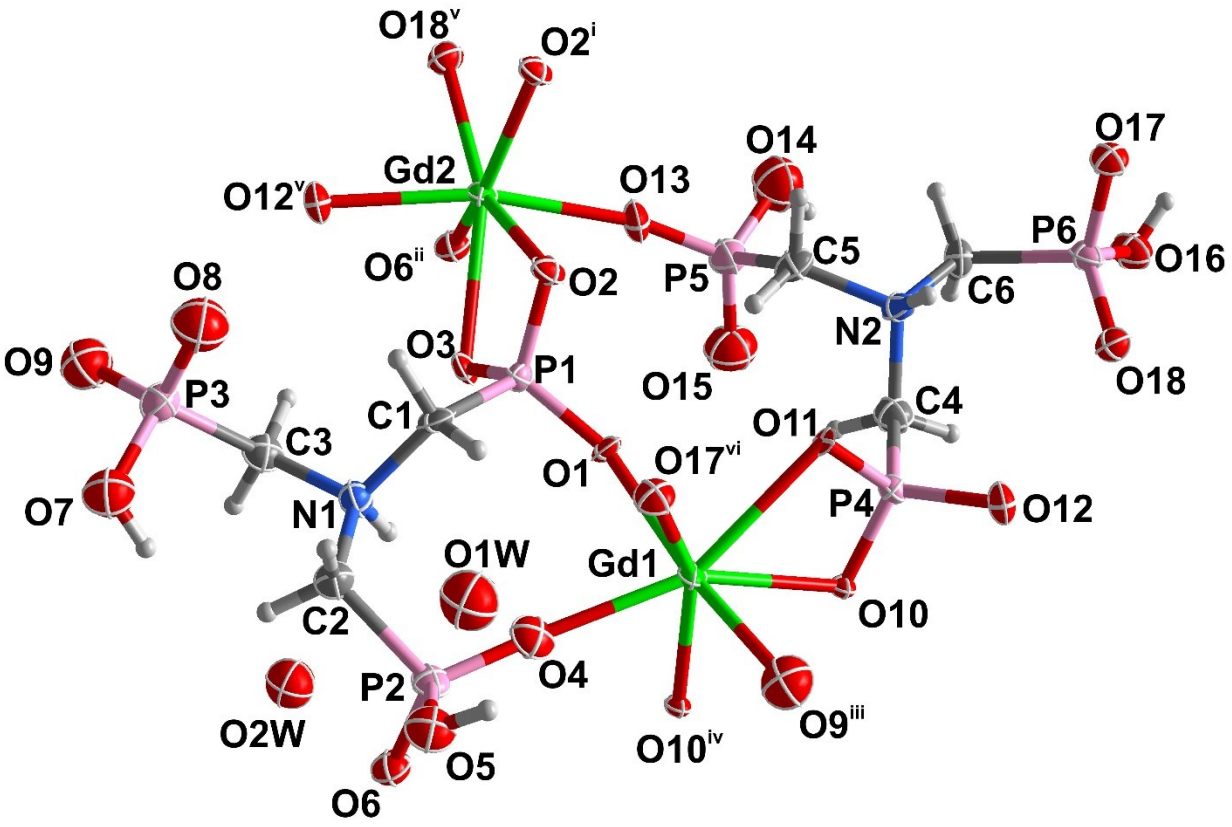

Figure S4. Asymmetric unit of $[Gd_2(H_3nmp)_2]\cdot 1.4H_2O$ (**2sc**) showing all non-hydrogen atoms represented as displacement ellipsoids drawn at the 50% probability level and hydrogen atoms as small spheres with arbitrary radius. The coordination sphere of the two crystallographically independent metallic centers have completed for the sake of clarity. Symmetry codes used to generate equivalent atoms: (i) *-x, -y*+1,*- z*+1; (ii) *-x*+1, *-y*+1, *-z*+1; (iii) *x, y*+1, *z*; (iv) *-x*+1, *-y*+2, *-z*+1; (v) *x*, *y*-1, *-z*+1; (vi) *-x*, *-y*+2, *-z*+1.

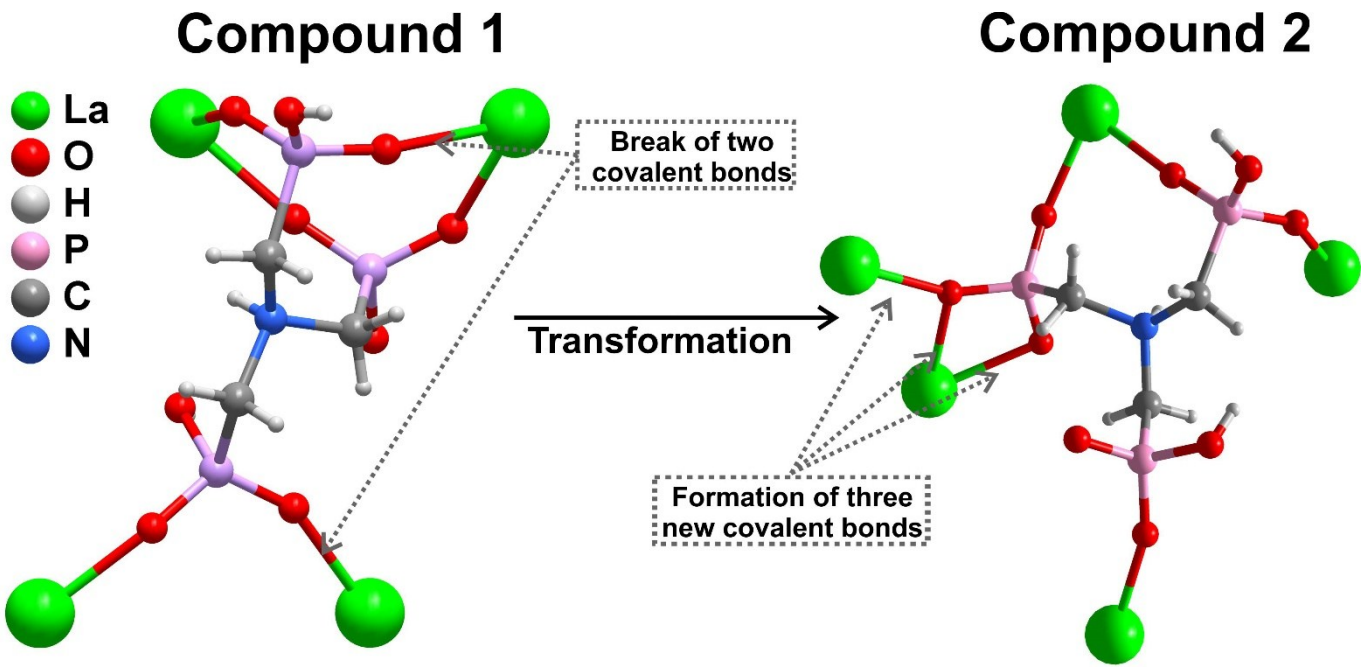

Figure S5. Schematic representation of the connectivity of the organic linker in $[Gd(H_4nmp)(H_2O)_2]Cl{\cdot}2H_2O$ (**1**) and in $[Gd_2(H_3nmp)_2]{\cdot}1.4H_2O$ (**2sc**).

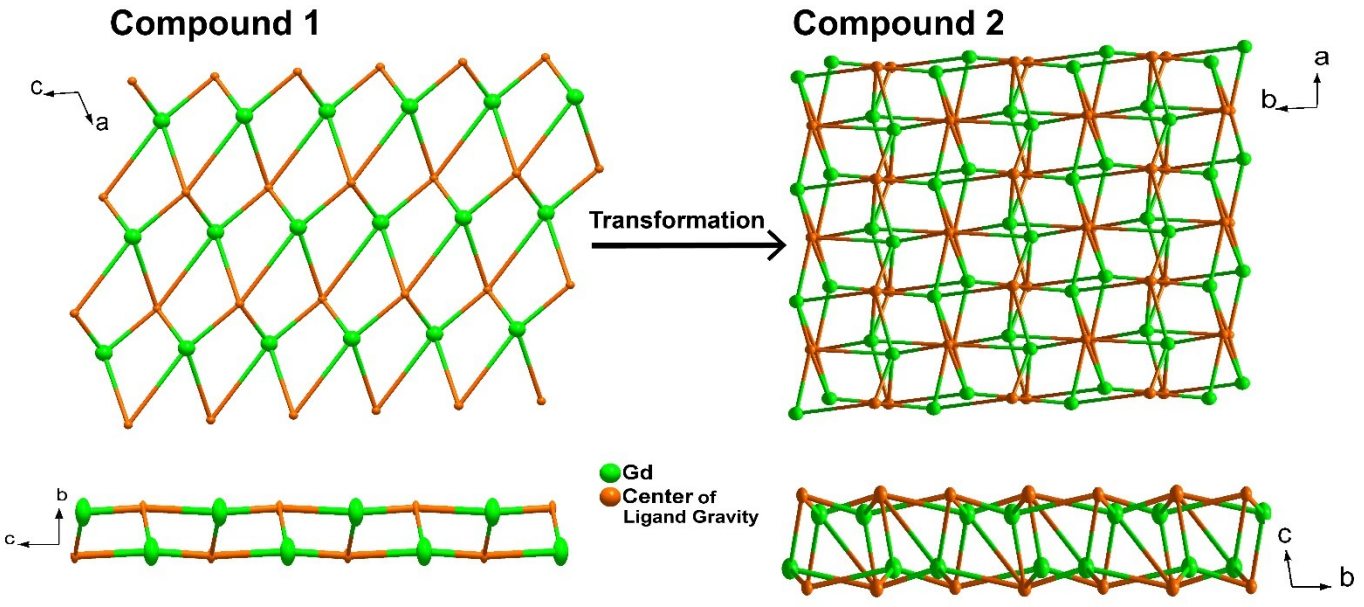

Figure S6. Schematic representation of the topological transformation of the anionic 2D layer in $[Gd(H_4nmp)(H_2O)_2]Cl{\cdot}2H_2O$ (**1**) to the neutral one in $[Gd_2(H_3nmp)_2]{\cdot}1.4H_2O$ **(2sc)** taking as nodes the metal center and organic linkers.

5. Protonic conductivity and water vapor sorption isotherms

5.1. Experimental

Proton conductivity (σ) of pelletized samples of **1** and **2** were studied by impedance spectroscopy. Disc shaped samples were obtained after pressing the powders in a uniaxial press at 6.25 MPa, and then isostatically at 200 MPa. The apparent density of these pellets was obtained from measurements of their weight and the geometric dimensions. Silver electrodes were applied on both sides of the pellets by painting a commercial paste (Agar Scientific). Samples were placed on ceramic tubular sample holders (equipped with platinum wires for current collection) inside a climatic chamber (ACS DY110) in order to carry out the measurements under variable temperature (40-94 °C) and relative humidity (RH, 20-98%). The impedance spectra were collected between 20 Hz and 2 MHz with test signal amplitude of 100 mV using an Agilent E4980A LCR meter. Spectra were analyzed with ZView (Version 2.6b, 1990–2002, Scribner Associates) to assess the ohmic resistance (R) of the pellets, which was normalized to the geometry of the samples to calculate the conductivity using the formula $\sigma = L(RA)^{-1}$, where L is the thickness of the pellets and A is the surface area of the electrodes. Before the measurements, the pellets were pre-treated overnight at 120 °C. Conductivity measurements were firstly carried out with increasing temperature (1st run) under a fixed humidity condition, and then during cooling down (2nd run). The samples were kept a 98% RH between the end of the 1st run and the beginning of the 2nd run. After the 2nd run and drying at 120 °C overnight, the pellet of **1** was submitted to a 3rd run of measurements at constant 98% RH. The activation energy (E_a) for the conductivity was obtained by fitting the data to the usual Arrhenius equation $\sigma=\sigma_0 T^{-1}\exp[-E_a(RT)^{-1}]$, where T is temperature (in Kelvin), σ_0 is a preexponential term and R is the gas constant (8,314 $Jmol^{-1}K^{-1}$).

The water vapour sorption isotherms were taken in a Dynamic Vapor Sorption apparatus from Surface Measurements Systems, using N_2 as the carrier gas (Air Liquide Alphagaz, less than 3 ppm H_2O, total flow of 200 sccm). Dry aliquots (*ca.* 20 mg) were loaded in a steel pan and suspended in the measuring chamber. The experiment started with a 2h pre-treatment at 150 ºC, to completely dry the sample, followed by the isotherm at 25 ºC with increasing and decreasing RH steps from 0 to 98 %. Each humidity step was kept until the rate of change of mass per fixed time (dm/dt) was lower than 0.002%, for a period of at least 10 min. As for the conductivity, two sets of measurements were also carried out for **1**, one for the pristine powder and a repetition of the after drying the powder overnight at 120 °C.

5.2. Protonic conductivity and water sorption Studies

Figure S6a shows Nyquist plots obtained at 80 ºC under variable RH conditions, normalized to the maximum in Z' for comparison purposes. The plots for RH equal or lower than 80% depict a single

semicircle, with amplitude corresponding to the bulk resistance of the sample. A simple equivalent circuit model, comprising a resistor in parallel with a These spectra can be easily fitted with a parallel circuit comprising a resistor in parallel with a constant phase element (R||CPE). The CPE impedance is defined as $Z_{CPE}=[Y_0(\omega)^n]^{-1}$, where ω is the angular frequency and Y_0 and n are parameters characterizing the pseudo-capacitance and the phase angle, respectively. The capacitance in the case of the R||CPE circuit is given by $C=R^{1/n-1}Y_0^{1/n}$. This model shows that the capacitance C is in the range of 27-29 pF, which is a common figure for an ionic bulk relaxation and thus R was used to calculate the conductivity. Under nearly saturated conditions (98% RH) the shape of the semicircle changes substantially with temperature. At 40 ºC, the spectrum shows a well-defined semicircle at high frequency and a depressed semicircle at intermediate frequencies, strongly overlapping with a capacitive tail at low frequency (Figure S6b). The possible non-linear behaviour of the various contributions to the system impedance was assessed by performing measurements with variable AC test signal amplitude, as discussed in ref.[12] Figure S6b shows that at lower temperature both the intermediate frequency and specially the low frequency capacitive tail change with increasing applied voltage, whereas the high frequency contribution remains unaffected, thus revealing the ohmic behaviour expected for the bulk resistance of the material. These spectra are dominated by the intermediate and low frequency contributions that are ascribed to interfacial impedances, namely resulting from the electrode processes or the ionic exchange of chloride ions. The determination of R in these cases (e.g. Fig. S6b and Fig. S7) implies the deconvolution of the spectra through fits to an equivalent circuit comprising two or three (R||CPE) elements in series, where the R of the element with the highest relaxation frequency is taken as the bulk resistance of the sample used to compute the conductivity. Comparison of Figures S6b and S6c shows that the impedance associated to the low frequency process is significantly reduced at high temperature. In fact, increasing temperature shifts the entire spectra to higher frequencies, and the bulk relaxation is no longer observed. In these spectra, R is given by Z' at the high frequency intercepted with the real axis of the Nyquist plot (Figure S6c).

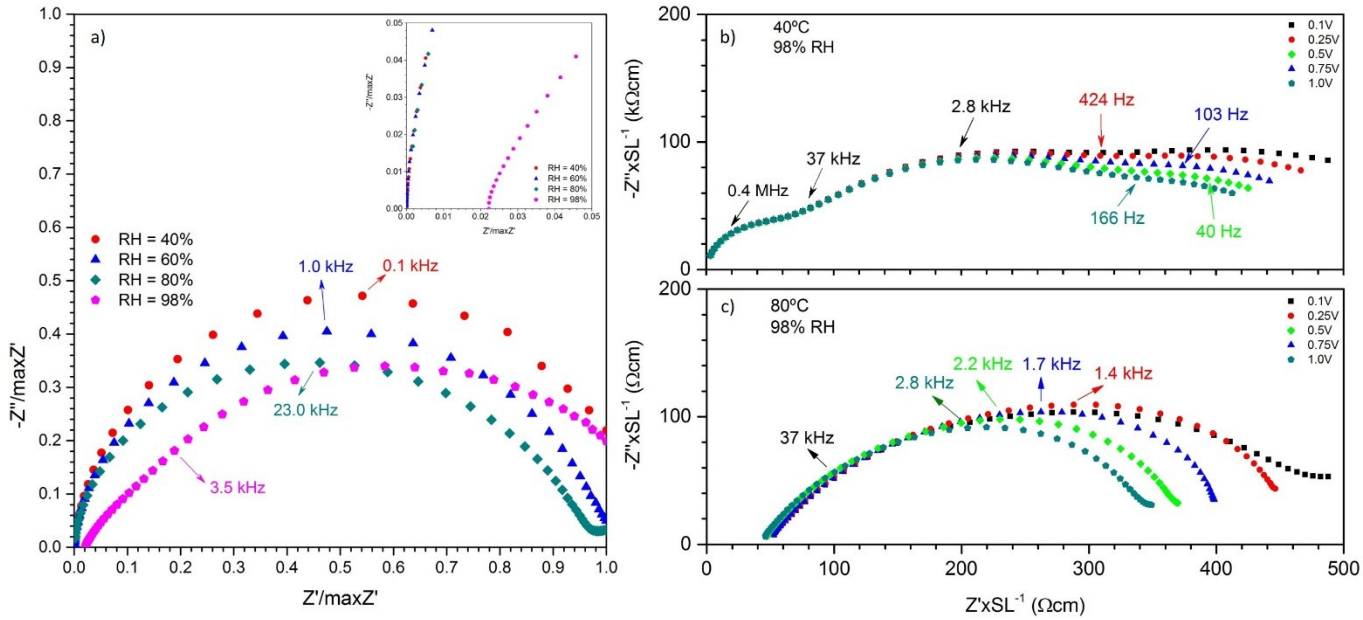

Figure S7. Nyquist plots for $[Gd(H_4nmp)(H_2O)_2]Cl{\cdot}2H_2O$ (**1**) in the 1st run, collected a) at 80 ºC under variable RH (V_{ac} = 0.1 V), b) at 98% RH and at 40ºC, and c) 98% RH 80 ºC under variable test signal amplitude.

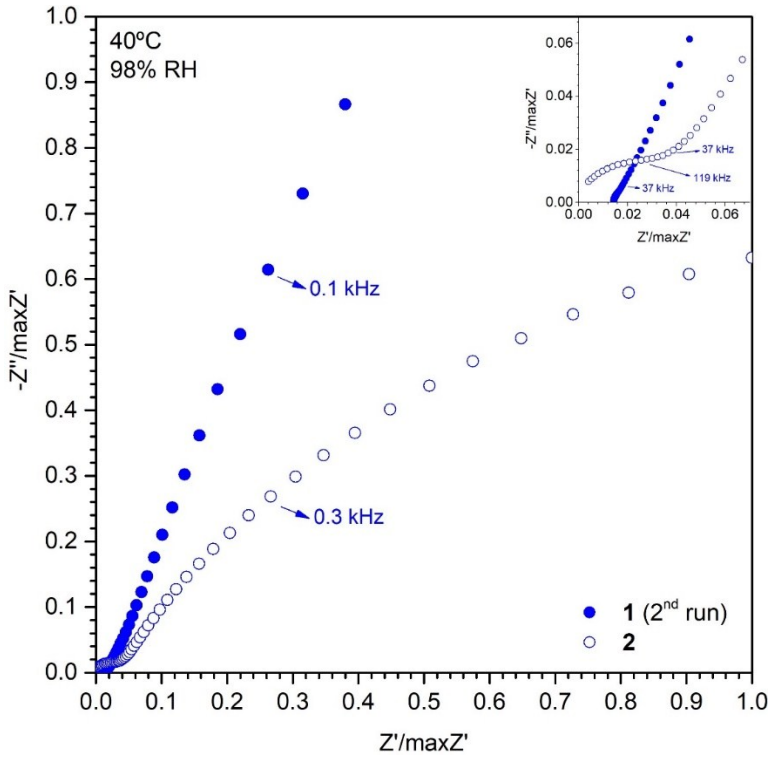

Figure S8. Nyquist plots for $[Gd(H_4nmp)(H_2O)_2]Cl{\cdot}2H_2O$ (**1**) in the 2nd run and $[Gd_2(H_3nmp)_2]{\cdot}xH_2O$ (**2**) (x = 1 to 4), collected at 40 ºC and 98% RH.

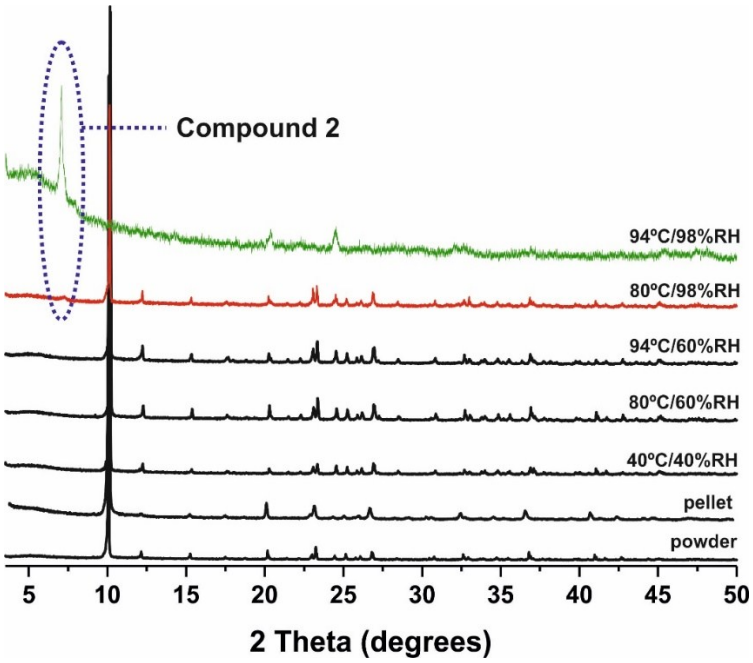

Figure S9. Powder X-ray diffraction of the bulk $[Gd(H_4nmp)(H_2O)_2]Cl{\cdot}2H_2O$ (**1**) when exposed to different RH and temperatures. The two top diffractograms emphasises the structural transformation into $[Gd_2(H_3nmp)_2]{\cdot}xH_2O$ (**2**) (x = 1 to 4).

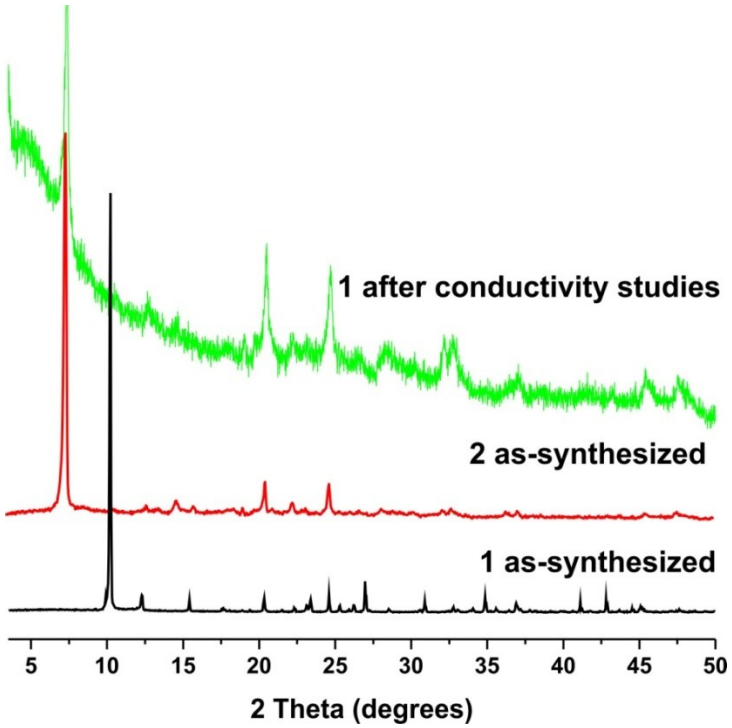

Figure S10. Powder X-ray diffraction of the pellet of $[Gd(H_4nmp)(H_2O)_2]Cl{\cdot}2H_2O$ (**1**) after conductivity measurements compared with that of as-prepared **1** and $[Gd_2(H_3nmp)_2]{\cdot}xH_2O$ (**2**) (x = 1 to 4).

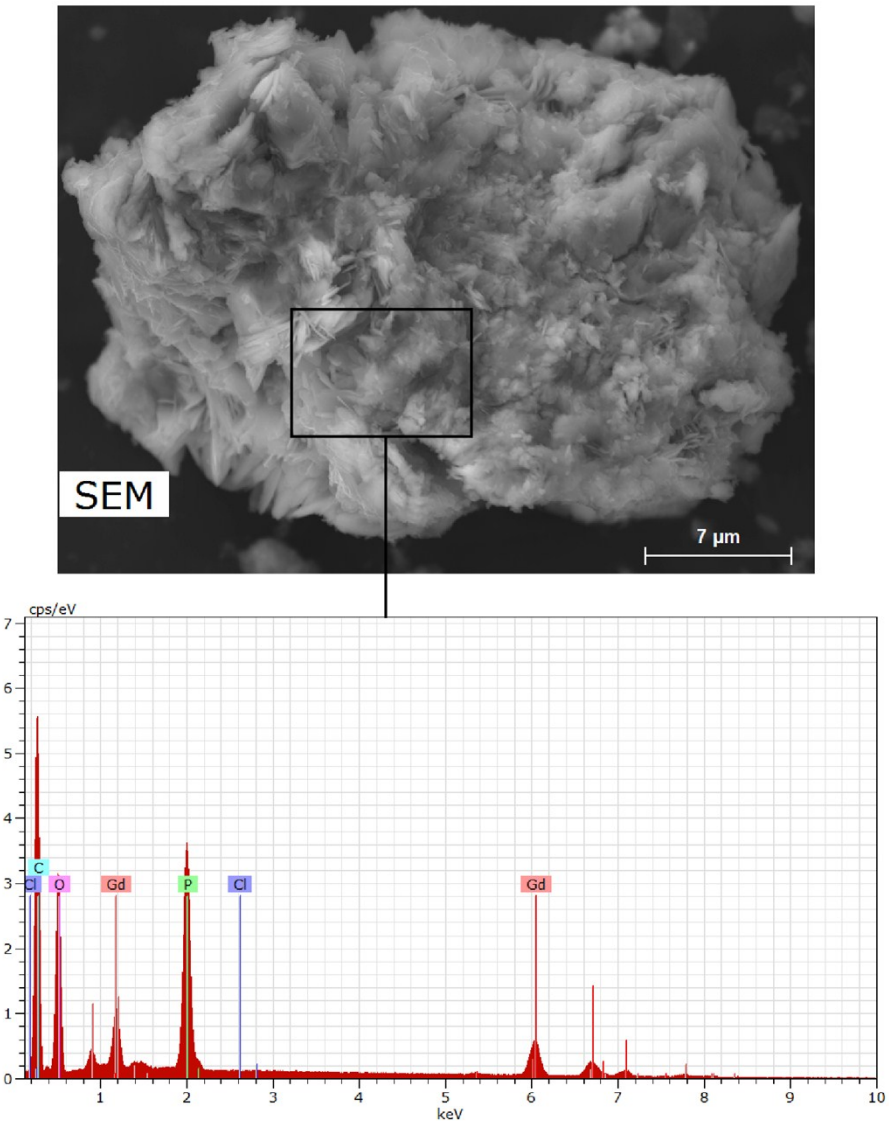

Figure S11. SEM image and EDS spectra of $[Gd_2(H_3nmp)_2]\cdot xH_2O$ (**2**) (x = 1 to 4) obtained in the transformation process, showing the absence of chloride ions in the sample.

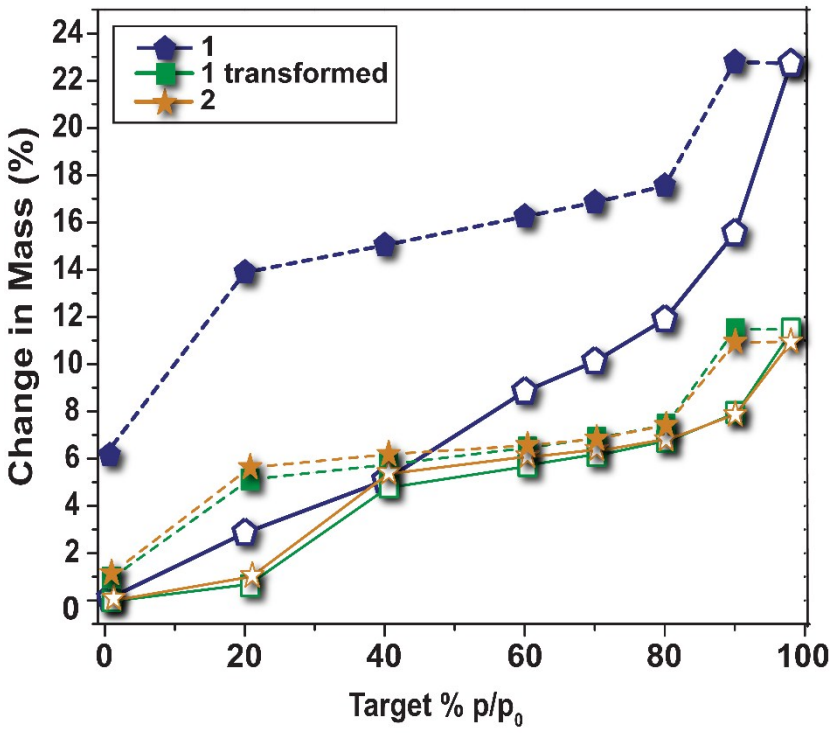

Figure S12. Water vapour adsorption isotherms measured at 25 °C of pristine (**1**) $[Gd(H_4nmp)(H_2O)_2]Cl{\cdot}2H_2O$ (**1**), a repetition of **1** after the first isotherm and drying overnight at 120 °C in dry conditions, and of as-synthesized $[Gd_2(H_3nmp)_2]{\cdot}xH_2O$ (**2**) (x = 1 to 4), where solid and dashed lines denoting adsorption and desorption cycles, respectively. Note the second isotherm of **1** is remarkably similar to that of **2**, indicating full transformation of **1** into **2** during the collection of the first isotherm of the as-prepared **1** powder.

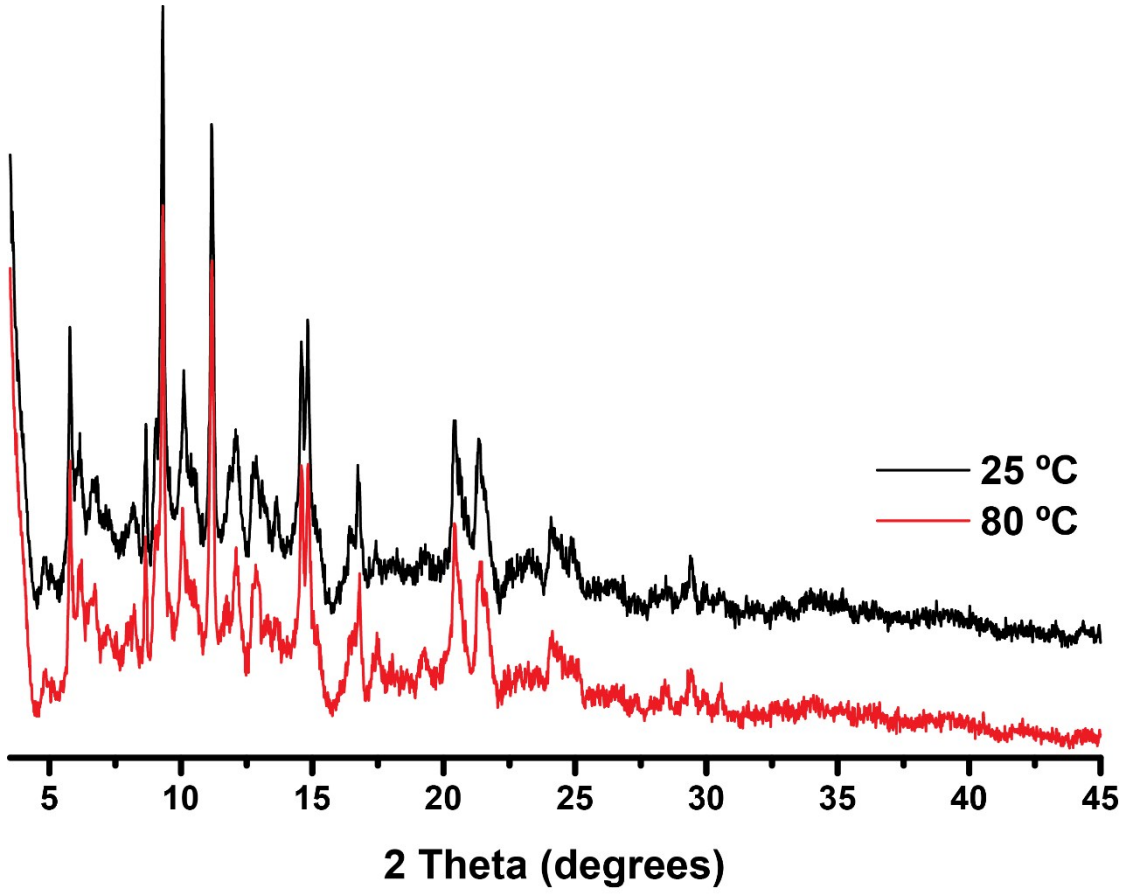

Figure S13. Powder X-ray diffraction of $[Gd_2(H_3nmp)_2]\cdot xH_2O$ (**2**) (x = 1 to 4) collected at 25 °C and 80 °C under constant 95% RH. *NOTE:* this powder X-ray diffraction was obtained with a molybdenum source.

Table S5. Activation energy (E_a) in kJmol^{-1} for the protonic conductivity of **1** measured under variable RH.

RH (%)	**20**	**40**	**60**	**80**	**98**
1st run	53	65	75	76	n.a.
2nd run	32	23	22	29	20

References

[1] R. F. Mendes, M. M. Antunes, P. Silva, P. Barbosa, F. Figueiredo, A. Linden, J. Rocha, A. A. Valente, F. A. A. Paz, *Chemistry-a European Journal* **2016**, *22*, 13136-13146.

[2] P. Silva, F. Vieira, A. C. Gomes, D. Ananias, J. A. Fernandes, S. M. Bruno, R. Soares, A. A. Valente, J. Rocha, F. A. A. Paz, *Journal of the American Chemical Society* **2011**, *133*, 15120-15138.

[3] T. Kottke, D. Stalke, *Journal of Applied Crystallography* **1993**, *26*, 615-619.

[4] APEX3, *Data Collection Software Version 2016.9-0, Bruker AXS, Delft, The Netherlands* **2005-2016**.

[5] Cryopad, *Remote monitoring and control, Version 1.451, Oxford Cryosystems, Oxford, United Kingdom* **2006**.

[6] SAINT+, *Data Integration Engine v. 8.37a*© **1997-2015**, Bruker AXS, Madison, Wisconsin, USA.

[7] L. Krause, R. Herbst-Irmer, G. M. Sheldrick, D. Stalke, *J. Appl. Crystallogr.* **2015**, *48*, 3-10.

[8] G. M. Sheldrick, *Acta Cryst. A* **2015**, *71*, 3-8.

[9] G. M. Sheldrick, *Acta Cryst. C* **2015**, *71*, 3-8.

[10] C. B. Hübschle, G. M. Sheldrick, B. Dittric, *J. Appl. Crystallogr.* **2011**, *44*, 1281-1284.

[11] K. Brandenburg, *DIAMOND, Version 3.2f. Crystal Impact GbR, Bonn, Germany* **1997-2010**.

[12] P. Barbosa, N. C. Rosero-Navarro, F. N. Shi, F. M. L. Figueiredo, *Electrochimica Acta* **2015**, *153*, 19-27.